Density of states determination in organic donor-acceptor blend layers enabled by molecular doping

Janine Fischer, Debdutta Ray, Hans Kleemann, Paul Pahner, Martin Schwarze, Christian Koerner, Koen Vandewal, and Karl Leo

Citation: Journal of Applied Physics **117**, 245501 (2015); doi: 10.1063/1.4922587
View online: http://dx.doi.org/10.1063/1.4922587
View Table of Contents: http://scitation.aip.org/content/aip/journal/jap/117/24?ver=pdfcov
Published by the AIP Publishing

Density of states determination in organic donor-acceptor blend layers enabled by molecular doping

Janine Fischer,[1,a)] Debdutta Ray,[1,2] Hans Kleemann,[3] Paul Pahner,[1] Martin Schwarze,[1] Christian Koerner,[1] Koen Vandewal,[1] and Karl Leo[1,b)]
[1]*Institut für Angewandte Photophysik, Technische Universität Dresden, 01062 Dresden, Germany*
[2]*Department of Electrical Engineering, Indian Institute of Technology Madras, Chennai 600036, India*
[3]*Novaled GmbH, Dresden, Germany*

(Received 30 April 2015; accepted 4 June 2015; published online 24 June 2015)

Charge carrier transport is a key parameter determining the efficiency of organic solar cells, and is closely related to the density of free and trapped states. For trap characterization, impedance spectroscopy is a suitable, non-invasive method, applicable to complete organic semiconductor devices. In order to contribute to the capacitive signal, the traps must be filled with charge carriers. Typically, trap filling is achieved by illuminating the device or by injecting charge carriers through application of a forward bias voltage. However, in both cases, the exact number of charge carriers in the device is not known and depends strongly on the measurement conditions. Here, hole trap states of the model blend layer ZnPc:C_{60} are filled by weak p-doping, enabling trap characterization in a blend layer at a controlled hole density. We evaluate impedance spectra at different temperatures in order to determine the density of occupied states (DOOS) directly from the capacitance-frequency spectra by assuming a simple energy diagram. The reconstructed DOOS distribution is analyzed at different doping concentrations and device thicknesses and compared to thermally stimulated current measurements performed on the same devices. In both methods, a pronounced Gaussian peak at about 0.4 eV below the transport level is found as well as deep, exponential tail states, providing a deeper insight into the density of states distribution of this donor-acceptor blend layer. Additionally, the effect of doping-induced trap filling on the solar cell characteristics is studied in these devices. © *2015 AIP Publishing LLC*. [http://dx.doi.org/10.1063/1.4922587]

I. INTRODUCTION

Although the principle of donor-acceptor blend layers for efficient exciton separation in organic solar cells is known for more than 20 years,[1,2] the processes limiting charge carrier transport are still under debate.[3,4] In addition to the generally low charge carrier mobilities of organic semiconductors, charge carrier transport and collection in blend layers can be additionally hampered by a reduced amount of available percolation pathways,[5] increased recombination,[6–9] as well as density of states (DOS) modifications caused by morphological changes as compared to neat materials.[4] Furthermore, the mobility of organic semiconductors depends on the electric field and/or the charge carrier density.[10–12] The latter relies on the DOS distribution, which is often assumed to be a Gaussian or exponential function of the energy.[13] Knowledge of the DOS distribution is crucial for understanding the transport properties of donor-acceptor blend layers.

Experimental determination of the DOS distribution is challenging, though various methods are available. Ultraviolet photoelectron spectroscopy (UPS) measures the energy resolved spectrum of electrons released upon excitation by UV radiation, yielding the density of occupied states (DOOS) distribution at low binding energies. Such spectra have previously revealed the presence of intra-gap states (traps).[14,15] However, the density of the trap states is often below the detection limit and results obtained with this technique refer to the surface of an excited sample. Another method is the measurement of thermally stimulated currents (TSCs), in which the sample is cooled to cryogenic temperatures and trap states are filled by a voltage and/or illumination pulse. Subsequently, charge carriers are released by increasing the temperature under reverse voltage.[16,17] However, this method only allows the characterization of shallow states in organic semiconductors with $\lesssim$0.4 eV energetic distance to the transport level and requires a transport model for extracting the charge carrier density and DOS distribution.[18,19] Moreover, space-charge limited current (SCLC) measurements of unipolar devices also reveal information on the DOS,[20,21] however, determining a complicated DOS distribution composed of several trap distributions is not unambiguously possible due to the amount of free parameters involved.

Impedance spectroscopy (IS) is well suited for characterizing trap states in fully functional solar cells under equilibrium conditions.[22,23] The challenge is to relate the measured capacitance-frequency spectra $C(\omega)$ to the DOOS distribution. When the energy level diagram of the device is known in the direction perpendicular to the substrate plane, the capacitive contribution of a trap can be calculated at each position in the device, and the DOOS distribution is obtained by fitting the $C(\omega)$ spectra, assuming a certain trap distribution.[24] However, it is not possible by this method to clearly assign the DOS to either charge carrier type. Even more interesting is the reverse approach, which provides direct access to the energetic

a)janine.fischer@iapp.de
b)leo@iapp.de

distribution of the DOOS by assuming a simple energy level diagram.[25] That way the DOOS can be directly determined from C-ω spectra. This method has recently been applied to air-exposed (oxygen-doped) P3HT-PCBM solar cells for characterizing trap states related to the presence of oxygen.[26] Nevertheless, this method has rarely been applied to organic semiconductors and a comparison to other DOS extraction methods on the same device has not been made, yet.

In this contribution, the DOOS distribution is determined for a model blend layer for vacuum processed small molecule organic solar cells, ZnPc:C_{60} (1:1), which is additionally p-doped by a strong acceptor complex. The use of vacuum processing allows doping of this material system in a reliable and controlled way. In this way, the Fermi level E_F is shifted towards the HOMO and holes are generated in the ZnPc phase, which fill up trap states. Hence, the IS signal can be attributed to holes only. In contrast, previous IS studies on blend layers used illumination or charge carrier injection (forward bias) in order to fill trap states. Thus, it was not possible to distinguish electron and hole traps because both charge carrier types contribute to the capacitance signal.[23] Here, UPS measurements are performed for determination of the Fermi level position, enabling insight into the energy level alignment. The DOOS is calculated from temperature dependent C-ω spectra by applying the Walter method,[25] the basics of which are presented in the Appendix. To obtain the necessary parameters, the following procedure is carried out:

(1) Record the temperature dependent $C(\omega)$ spectra and derive the depletion width d from the trap capacitance C_t at low frequencies.
(2) Determine the characteristic trap frequency ω_0 from the trap conductance $G_t(\omega)$ and extract the attempt-to-escape frequency ν_0 from the T dependence of ω_0 according to Eq. (A4).
(3) Determine V_d from a Mott-Schottky analysis and E_F from UPS measurements to determine the energy level diagram.
(4) Evaluate the DOOS reconstruction at different doping concentrations and intrinsic layer thicknesses.

The parameters and the related uncertainties in the reconstruction are discussed in detail. Moreover, TSC measurements are performed in order to confirm the features found in the reconstructed DOOS distribution. Additionally, the J-V curves of the illuminated devices (i.e., the solar cell characteristics) are shown to be hampered by the trap filling in thick and highly doped blend layers, which is caused by a reduction of the depletion zone necessary for charge carrier separation. By comparing the DOOS to previous results obtained for ZnPc:C_{60} blend layers, a conclusive picture on the hole DOS of this prototype donor-acceptor blend system is developed.

II. METHODS

The p-doped bulk heterojunction layers are thermally evaporated under high vacuum conditions (base pressure $<10^{-8}$ mbar) using a wedging tool (Kurt J. Lesker Company) in order to ensure the comparability of the devices. In particular, equal weight ratios of zinc phthalocyanine as donor (ZnPc) and fullerene C_{60} as acceptor (both from CreaPhys) are co-deposited with the p-dopant $C_{60}F_{36}$ (Ionic Liquids Technologies GmbH) in weight ratios of 0.25 and 0.5 wt % with respect to ZnPc (i.e., 0.07 and 0.13 mol. % relatively to the whole blend). The triple blend layer is deposited on indium tin oxide (ITO, anode) coated glass substrates in layer thicknesses L of 100 nm and 200 nm with an estimated relative uncertainty of 10% in layer thickness and doping concentration. The devices are finished by a 100 nm layer of aluminum serving as the cathode. Subsequently, the devices are encapsulated. All samples have an active area of $A = 6.44\,mm^2$. An undoped sample serves as reference sample.

IS measurements are performed using an Autolab PGSTAT302N in an evacuated Peltier-heatable and -coolable chamber that allows for temperature variations from about $-50\,^{\circ}C$ to $50\,^{\circ}C$. Capacitance-frequency spectra $C(\omega)$ are taken at 0 V bias voltage from 1 to 10^6 Hz using a signal amplitude of 20 mV. C-V sweeps are taken from -1 to 0.5 V at a frequency of 100 Hz.

For *in situ* UPS measurements, p-doped ZnPc:C_{60} blend layers with a layer thickness of 30 nm are thermally co-evaporated on solvent cleaned and ozone treated ITO. The doping ratios are 0.25 and 0.5 wt %, controlled by rate monitors and a rotating shutter (see also Ref. 27). Subsequently, the samples are transferred into the UPS analysis chamber without breaking the ultra-high vacuum (base pressure: 10^{-11} mbar). UPS spectra are acquired by a PHOIBOS 100 system (SPECS GmbH) using the He I (21.22 eV) excitation line and calibration to the Fermi level position of a sputter cleaned gold foil.

TSC measurements are performed on the devices as used for IS using a JANIS STVP-100 continuous flow cryostat. Before the measurement, the encapsulation is removed from the samples and they are immediately transferred to the cryostat, where they are kept in inert atmosphere at all times to prevent possible degradation. Trap filling is realized electrically by driving the samples at the load temperature of 10 K for 1 min in forward direction. Due to expected recombination losses in the ambipolar sample structures, a number of consecutive TSC experiments are carried out in order to obtain the minimal necessary loading current, i.e., to see a saturation of the trap level signal. After trap filling and a rest time of 5 min, the TSC measurements are performed with a linear heating rate of 5 K/min. The released charge carriers are extracted by the built-in voltage of the samples, and the current (TSC) is measured with a KEITHLEY 2635 A femto amp source meter.

III. RESULTS AND DISCUSSION

A. Impedance spectroscopy

Frequency-dependent capacitance measurements $C(\omega)$ are carried out in order to determine the capacitive contribution of charge carriers upon application of a small perturbation signal at different temperatures. The molecular structures of the used materials are presented in Figure 1(a) and the device stack in Figure 1(b). Figures 1(c)–1(g) show the measured spectra of the capacitance $C(\omega)$ and the

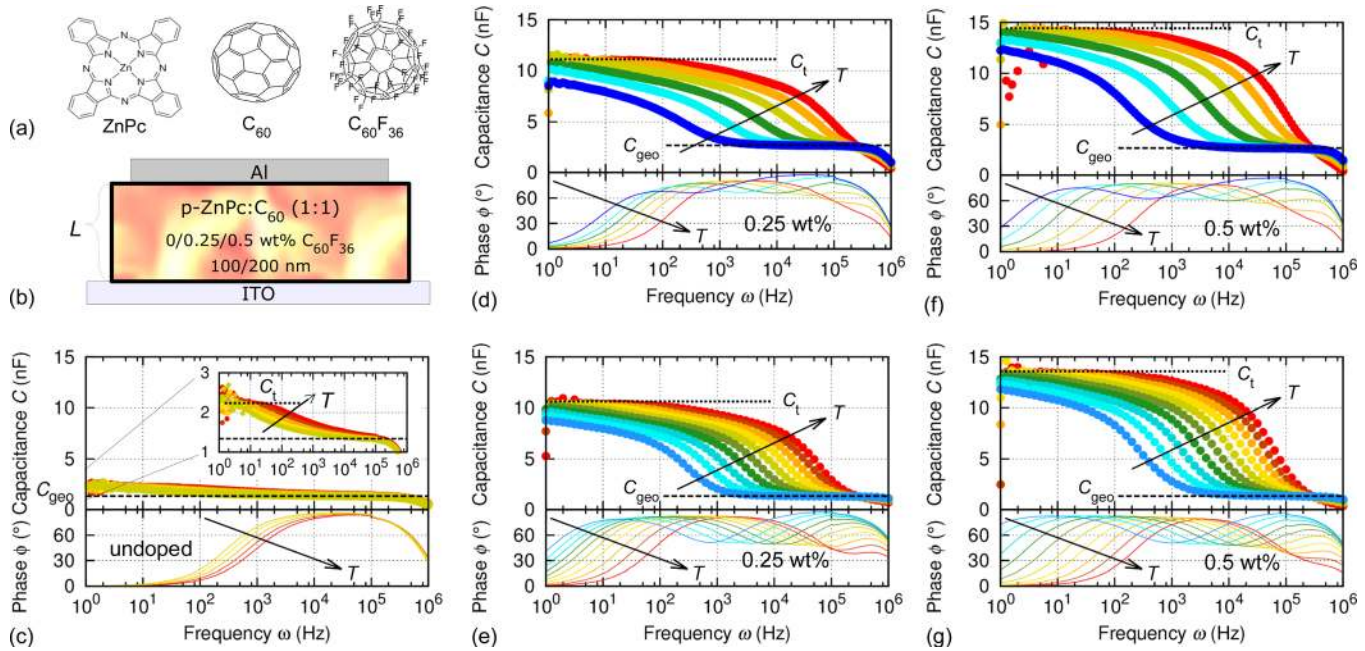

FIG. 1. Temperature dependent impedance spectra of devices using the molecules sketched in (a) and the device stack shown in (b): $C(\omega)$ data and absolute value of the phase for (c) undoped blend layer (200 nm layer thickness), (d) and (e) 0.25 wt % p-doped blend layers (100 nm and 200 nm, respectively), as well as (f) and (g) 0.5 wt % p-doped blend layers (100 nm and 200 nm, respectively). Equal colors represent equal temperatures from 223 K to 323 K (10 or 20 K steps). The according geometrical capacitance C_{geo} (calculated using $\varepsilon = 4.7$) is indicated by the dashed line and the saturated trap capacitance C_t by the dotted line.

absolute value of the phase $\phi(\omega)$ for devices with varying doping concentration from 0 to 0.5 wt % doping and with a layer thickness L of 100 nm and/or 200 nm (see Figure 1(a)).

For the undoped blend layer, the $C(\omega)$ spectra are governed by the geometrical capacitance C_{geo}, which describes the data well using $\varepsilon = 4.7$. The small additional capacitive contribution at low frequencies can be related to a few charge carriers occupying trap states that are mostly empty. It compares with previous impedance measurements performed on this blend layer in a similar m-i-m structure.[24] This device is not further evaluated, here. For the doped devices, all $C(\omega)$ spectra have a similar shape: From high to low frequencies, C is governed by the serial resistance ($\omega > 3 \times 10^5$ Hz), reaches a plateau at the geometrical capacitance of the device C_{geo} (for $\omega < 3 \times 10^5$ Hz, low temperatures), and increases further due to an additional trap response. Finally, the spectra saturate at a capacitance C_t in addition to C_{geo} at low frequencies (for $T \geq 263$ K). The transition from C_{geo} to the low frequency plateau is shifted to lower frequencies for decreasing T, indicating a temperature dependent occupation of the traps.

The trap capacitance observed in the doped devices is characteristic for a depletion region, where charge carriers can only be trapped and released at low frequencies, but not at high frequencies when the whole device is completely depleted ($C(\omega) = C_{geo}$). In other words, the trap capacitance describes the slow charge carriers that require a certain activation (thermal activation through high T or electrical activation at low frequencies ω) to contribute to the device capacitance. Hence, the trap capacitance is a depletion capacitance in the part of the device, where the charge carriers are trapped.

The trap capacitance C_t of these devices is evaluated in terms of a depletion region in Table I. Theoretically, the capacitance of a depletion region should not depend on the device thickness and should increase by $\sqrt{N_A^-}$ with the dopant density (i.e., a factor of $\sqrt{2}$ difference between 0.25 and 0.5 wt % when the doping efficiency is approximately assumed equal). Within the experimental error, the capacitance values of Table I at a constant doping concentration are equal for different thicknesses (deviations are smaller than 1 nF or 10%). Comparing the different doping ratios, the devices with higher doping ratio also have a larger trap capacitance as expected (by a factor of 1.37 for the 100 nm devices and 1.33 for the 200 nm devices). In contrast to the undoped samples, a trap capacitance saturating at low frequencies is observed in the doped samples, which is increasing with increasing doping concentration indicating trap filling by doping.

The temperature dependence of the transition from C_{geo} to C_t is caused by a temperature dependent activation of traps. As explained in the Appendix, this transition can be

TABLE I. Trap capacitance C_t obtained from the low frequency regime of $C(\omega)$ (plateau value less C_{geo}) and the according depletion width d assuming a plane capacitor and a permittivity of $\varepsilon_r = 4.7$ for the doped devices of Figure 1.

Doping (wt %)	L (nm)	C_t (nF)	d (nm)
0.25	200	9.1	29.4
0.5	200	12.1	22.1
0.25	100	8.3	32.2
0.5	100	11.4	23.5

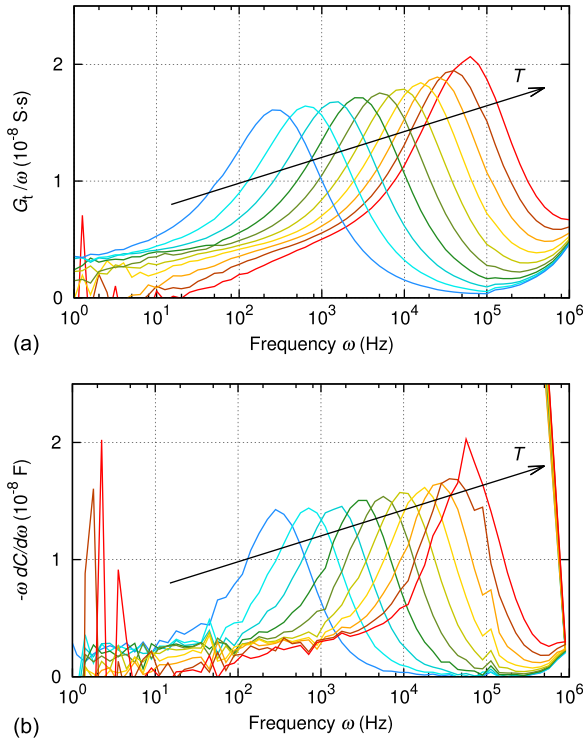

FIG. 2. Frequency dependence of the trap contribution to the conductance G_t/ω and the capacitance change $-\omega dC/d\omega$ for the 200 nm device with 0.25 wt % doping for different temperatures ($T = 234 - 324$ K).

used to determine the attempt-to-escape frequency ν_0 from the emission frequency ω_0 of a charge carrier trapping process. In order to do that the frequency ω_0 of the maximum in the trap conductance $G_t(\omega)/\omega$ is evaluated at different temperatures. Equivalently, ω_0 might be obtained from $-\omega dC/d\omega$ as both representations physically contain the same information. Figure 2 shows the spectra obtained from both methods. However, the results are less reliable for the $-\omega dC/d\omega$ signal since the derivative $dC/d\omega$ is used. Therefore, the frequency of the maximum ω_0 is determined from the $G_t(\omega)/\omega$ spectra in the following.

In Figure 3, the obtained ω_0 values are plotted against inverse temperature for all doped devices. The activation energy E_A, i.e., the energy between the trapped charge carrier and the transport level, as well as the attempt-to-escape frequency ν_0 are obtained by fitting the data with Eq. (A4). The four devices under investigation have similar activation energies of (0.41 ± 0.01) eV, whereas the attempt-to-escape

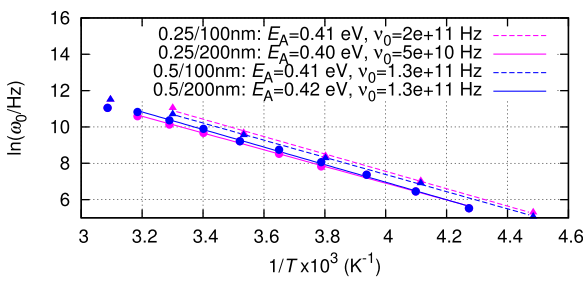

FIG. 3. Arrhenius plot the determined frequencies ω_0 of the maximum in the $G_t(\omega)/\omega$ spectra for devices with different doping concentrations (0.25 and 0.5 wt %) and thicknesses (100 and 200 nm).

frequencies ν_0 range from 5×10^{10} Hz to 2.0×10^{11} Hz. The accuracy of this fit is dominated by the uncertainty in ω_0, which is limited by the size of the frequency steps. Here, the frequency steps are smaller for the 100 nm devices resulting in a better accuracy. Within the resolution limit, a trend for ν_0 and E_A cannot be observed. Hence, ν_0 is considered a constant material parameter and is averaged over all samples to $\nu_0 = 1.3 \times 10^{11}$ Hz, in agreement with the values assumed in the literature.[23,28–30]

B. Fermi level, Mott-Schottky analysis, and energy level diagram

In order to relate the measured capacitance spectra to a DOOS distribution, the potential drop over the depletion region V_d is required (see also Fig. 5). Therefore, the energy level diagram is determined from the Fermi level position in the doped blend layer and the built-in voltage of the device. The latter is obtained from a Mott-Schottky analysis and the Fermi level from UPS measurements.

From the UPS spectra at room temperature, the Fermi level is determined to be at 4.35 and 4.42 eV below the vacuum energy for the 0.25 and 0.5 wt % doping concentration, respectively. Compared to the value obtained for undoped blend layers before (4.33 eV),[31] the Fermi level of the 0.25 wt % doped sample obtained here is very similar. Thus, such low doping does not significantly influence the Fermi level position, probably because the defect density in the blend is similar to the doping concentration (see Sec. III C), so that holes generated by doping are filling up trap states first. In the 0.5 wt % sample, the Fermi level is already shifted by 0.09 eV as compared to the undoped blend, indicating the generation of free holes by doping. For all doping concentrations, the according values of the ionization potential (IP) are equal (5.14 eV for doped samples and 5.12 eV for undoped blend layers[31]) within the measurement accuracy ($\approx$0.05 eV), even though the value for the undoped blend has been measured on a gold substrate.

Interestingly, the Fermi level position within the energy gap of the undoped/weakly doped sample is *not* in the center of the effective gap given by the electron affinity (EA) of C_{60} EA(C_{60}) = 4.0 eV[32] and IP(ZnPc) = 5.14 eV as expected for an intrinsic semiconductor. Instead, it is located close to EA(C_{60}) and the semiconductor seems rather n-type. However, doping the blend by $C_{60}F_{36}$ shifts the Fermi level closer to IP(ZnPc), indicating the generation of free holes. Thus, it can be concluded that p-doping works as expected. A possible origin for the asymmetry in the Fermi level position may be a large difference in the effective density of states of ZnPc and C_{60}, i.e., a large difference between electron and hole density that are able to contribute to charge carrier transport (N_V/N_C would be 7×10^{-5} in order to account for the measured Fermi level position of the undoped device).[33] However, this estimation assumes the transport level to be at the band edge, which is not true for organic semiconductors. It will be shown in the following that the hole transport level is located deep within the energy gap as compared to IP(ZnPc), forcing the Fermi level position closer to EA(C_{60}). Altogether, the shift of the transport

level as well as the Fermi level can be attributed to deep hole trap states.

In the following, $C(V)$ measurements are performed in order to determine the built-in voltage of the device V_{bi}. Additionally, the number of ionized dopants N_A^- is analyzed for different temperatures from a Mott-Schottky analysis as presented in Figure 4. The inset shows the temperature activation of N_A^- for the 0.5 wt % doped sample, which has an activation energy of $E_{A^-} = 44$ meV ($E_{A^-} = 31$ meV for 0.25 wt %, not shown). Comparing the room temperature values of N_A^- to the intended dopant density in the device leads to a doping efficiency of 23% (28%) in the ZnPc:C_{60} matrix for a doping ratio of 0.5 wt % (0.25 wt %). Assuming a uniform distribution of dopants in the blend and considering that the dopant is not expected to dope C_{60} ($EA(C_{60}F_{36}) = 5.4$ eV[34] and $IP(C_{60}) = 6.4$ eV), the real doping efficiency in the ZnPc phase is actually higher by a factor of 2, i.e., 46% (56%), respectively. In this regard, the doping efficiencies compare well to those obtained for donor materials with the same IP and doped with the same dopant (pentacene[35] or MeO-TPD[36]). Hence, it seems that the doping of a donor-acceptor blend layer works in the same way as in neat layers.

The built-in potential of the device V_{bi} is obtained from the Mott-Schottky plots to be 0.5 ± 0.1 V for both doping concentrations. It determines the work function difference of the ITO and the Al contact. Using the Fermi level position of the blend layer known from UPS measurements, the energy level diagram results as demonstrated in Figure 5: At the Al contact, a hole depletion region forms, where doping-induced holes are trapped in deep states dominating the $C(\omega)$ spectra at low frequencies. Hence, the potential drop over the depletion region V_d is given by $eV_d = |E_F - \phi(\mathrm{Al})|$. Table II summarizes the values obtained for V_d. The uncertainty in V_d is mainly caused by the uncertainty of the UPS measurement (0.05 eV). Furthermore, there is a hole accumulation zone for holes at the ITO contact V_{acc}, which is thin and highly conductive. It does not influence the evaluation of the $C(\omega)$ spectra. Instead, the spectra are dominated by the capacitance of the extended depletion region V_d.

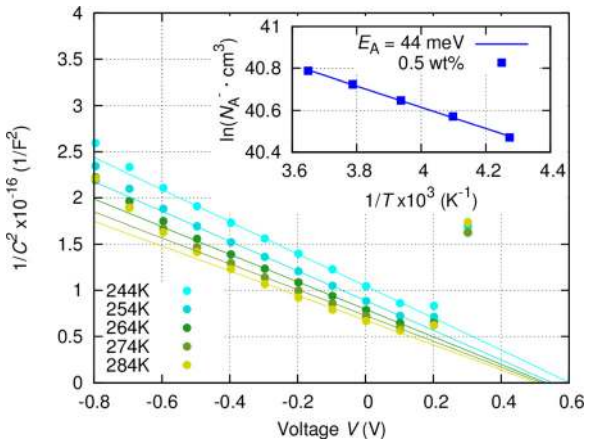

FIG. 4. Temperature dependent Mott-Schottky analysis for a doping concentration of 0.5 wt %, $L = 200$ nm, and $\omega = 100$ Hz. Inset: temperature activation of the density of ionized dopants and the according activation energy resulting from an Arrhenius fit of the data.

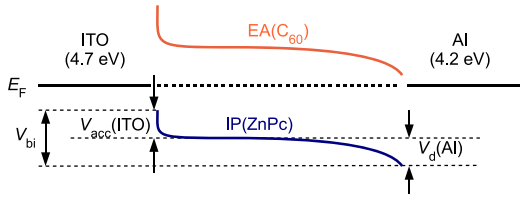

FIG. 5. Schematic energy level diagram at 0 V: The effective energy levels of the semiconductor are given by the electron affinity of C_{60} (4.0 eV) and the ionization potential of ZnPc (5.14 eV), the ITO workfunction results from V_{bi}, and the Fermi level position from UPS measurements. The dominant capacitance is caused by the depletion region at the Al contact, whereas there is an accumulation region at the ITO contact. It is shown later that the hole transport level is located around 4.7–4.8 eV, i.e., significantly above the HOMO level.

C. DOOS determination

The DOOS distribution $N_t(E_\omega)$ is reconstructed from the $C(\omega)$ spectra at different temperatures using Eqs. (A5) and (A8) with the parameters determined in Sections III A and III B. Here, a parabolic depletion region at the Al contact is assumed, which is justified since the Mott-Schottky plot shows a straight line.[37] In Figure 6, the obtained $N_t(E_\omega)$ spectra are shown for the devices with 100 nm and 200 nm organic layer at different temperatures (symbols) and with error bars (determined as explained in the following). As the capacitance is dominated by the hole depletion region at the Al contact, the distribution represents hole-type trap states and E_ω refers to the hole transport level.

Converting the frequency axis into the energy axis requires the knowledge of ν_0. If ν_0 is correct, the DOOS distributions of the same sample coincide for different temperatures.[25] Here, the good overlay of the spectra at different temperatures for all samples around the peak position indicates that ν_0 was correctly determined. The fitting errors of ν_0 (Figure 3) cause an uncertainty in the demarcation energy of $\Delta E_\omega = 0.73 \cdot kT$ (obtained from Gaussian error propagation). Furthermore, the uncertainty of the reconstruction in N_t is determined by the prefactor to $dC/d\omega$ in Eq. (A8), i.e., the assumed shape of the energy level diagram and the uncertainties to the used values. Here, only the uncertainty in V_d is accounted for and ΔN_t is calculated from a linear approximation of the Taylor expansion. Fluctuations in the region of deep states ($E_\omega > 0.45$ eV) originate from the $C(\omega)$ spectra at low frequencies having a low phase and small deviations in $C(\omega)$ are enhanced by taking the derivative $dC/d\omega$ as a linear interpolation between neighboring data points. In the 200 nm devices, the frequency steps are larger, causing more outlaying data points. For reducing the noisiest data, only data points with a minimum phase of 20° are used in the plots. Moreover, frequencies $\omega > 10^5$ Hz are excluded

TABLE II. Voltage drop at the depletion region V_d determined from the Fermi level E_F values obtained from UPS (with respect to the vacuum level) for the different doping ratios.

Doping (wt %)	E_F (eV)	V_d (V)
0.25	4.35	0.15
0.5	4.42	0.22

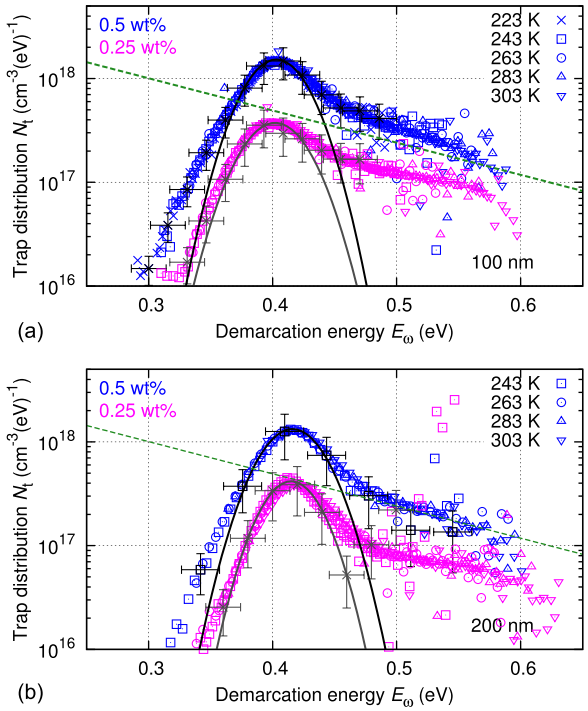

FIG. 6. Trap density reconstruction from $C(\omega)$ spectra of different temperatures (symbols) for the 100 nm and the 200 nm devices with error bars for selected data points. The peak positions are fitted with a Gaussian (solid lines) to estimate the involved charge carrier density. For comparison, the distribution of exponential tail states determined for this blend layer before[21] is shown (green dashed line).

from the evaluation in order to avoid artifacts from the serial resistance.

The resulting DOOS distribution describes the energetic distribution of the occupied states in the device, which is modified by changing the temperature and the perturbation frequency. In terms of energy, the DOOS reconstruction ranges from the Fermi level position (low demarcation energies) further into the energy gap (by the size of the energy level bending at the depletion region V_d). States that are deeper than V_d from the Fermi level as well as those above the Fermi level do not contribute to the $C(\omega)$ spectra and neither to the DOOS distribution because they cannot be (de-)occupied. Relating the energetic range to the Fermi level gives an estimate of the hole transport level position within the energy gap (here $\approx$4.7–4.8 eV from the vacuum level for all devices). Note that the uncertainty of V_d does not influence the energetic distribution of the spectra but only the vertical position, because it only influences the prefactor in Eq. (A8) and not Eq. (A5).

The DOOS reconstruction of all devices shows a peak at around 0.4 eV, which compares to the activation energy determined from the Arrhenius plot of ω_0 as expected. Fitting this peak with a Gaussian distribution gives the density of charge carriers producing this peak. Note that the data points further away from the peak center are broadened as compared to the Gaussian fit, which is also observed in the TSC measurements shown later in this work (Sec. III D). Here, the density of the Gaussian center of the peak is determined for simplicity. For both, the 100 and the 200 nm devices, the peaks of the 0.5 wt % devices (8.8×10^{16} cm^{-3} and 8.0×10^{16} cm^{-3}) comprise 3–4 times more charge carriers than those doped with only 0.25 wt % (2.3×10^{16} cm^{-3} for both L). As the densities at equal doping concentrations are the same for different thicknesses, it is confirmed that the measured trap capacitance refers to bulk traps. The difference in the charge carrier densities at different doping concentrations does not scale with the doping concentration, which may be explained by a different degree of trap filling. In particular, the holes generated by doping in the lower doped sample are required to fill up deeper trap states, whereas the additional dopants introduced at the higher doping concentration directly fill up the states of the Gaussian trap. Possible origins of this trap will be discussed in Sec. III F together with the results from the TSC measurements.

The deep energy part of the doped devices ($E_\omega > 0.45$ eV) shows lower N_t values representing an exponential tailing. At both layer thicknesses, there is an offset in N_t for the two doping concentrations, whereas the slope is the same. If these deep tail states are a property of the donor-acceptor blend and are not created by the presence of the dopant molecules, they should be occupied by doping and the tail state distribution should be the same for both concentrations. However, on the one hand, the offset can hardly be distinguished within the uncertainty of N_t (caused by V_d). On the other hand, keeping in mind that E_ω refers to the transport level, the apparent offset in N_t might as well be related to an offset in E_ω caused by a shift of the reference transport level at different doping concentrations. Assuming that the hole transport level shifts similarly to the Fermi level, the DOOS distribution of the 0.25 wt % sample would be shifted by about 0.07 eV to the right (not shown). Hence, the trap peak would shift to deeper energies (i.e., higher E_ω) and the exponential tail states would overlay for the two doping concentrations as expected. In future investigations, this interpretation might by related to transport level investigations, e.g., using Seebeck measurements.

Compared to previous results, the slope of the tail states (i.e., the characteristic trap energy $E_t = 0.14$ eV) compare nicely to the exponential tail state distribution determined for ZnPc:C$_{60}$ (1:1) blend layers before[21] (green dashed line). The according trap density is difficult to compare because it depends on the position of the transport level. Nevertheless, the agreement of the data to the previously determined tail state distribution is good. Furthermore, a Gaussian trap distribution obtained from IS measurements of p-i-n solar cells by Burtone *et al.*[24] ($N_G = 3.5 \times 10^{16}$ cm^{-3}, $\sigma_G = 0.055$ eV, and $E_G = 0.458$ eV) is also in the same order of magnitude as the DOOS reconstruction obtained here. Although the method for determination of the trap DOS was similar to the one used here (an energy level diagram was calculated using drift-diffusion simulations in order to fit the trap capacitance of an assumed trap distribution to the $C(\omega)$ spectra), it was not possible to distinguish between a Gaussian trap and exponential tail states, there. Consequently, that Gaussian distribution is broader than the peak obtained here and deeper in energy, whereas the center of the Gaussian compares to the center of the energy range accessed here. By using p-doping in the present work, the traps can be clearly attributed to holes, which was not possible in previous IS studies.

Altogether, the DOOS reconstruction presented here gives a closer insight into the DOS distribution of ZnPc:C_{60} blend layers and refines previous impedance investigations of deep intra-gap states.

D. Thermally stimulated currents

In order to validate the resulting trap distributions, the 200 nm thick samples are measured with TSC. Measured TSC spectra with and without electrical trap filling are plotted in Figure 7. Both doped samples show a pronounced peak at around 130 K, which can be attributed to a trap state that is not occupied without trap filling (compare thin solid lines). Furthermore, the peak position is shifted towards lower energies and has more charge carriers in the case of the 0.5 wt % sample as compared to 0.25 wt %. At $T > 150$ K, the samples start to release charge carriers, no matter whether the traps have been filled or not. This effect is attributed to a leakage current and not further evaluated.

For quantitative evaluation of the trap spectra, the model of Haering and Adams[16] is applied, describing the evolution of the TSC signal $I(T)$ according to

$$I(T) = A\frac{V_{bi}}{L} q\mu\tau\nu_0 \int_{-\infty}^{\infty} dE \cdot DOS(E) \times \exp\left[-\frac{E}{kT} - \frac{\nu_0}{\zeta}\int_{T_0}^{T} \exp\left(-\frac{E}{kT'}\right)dT'\right] \quad (1)$$

using the mobility μ, the charge carrier lifetime τ, the density of states $DOS(E)$, the heating rate $\zeta = 5$ K/min, as well as the starting temperature T_0. Related to the same trapping process, ν_0 is chosen in accordance with the previous results of the impedance measurement. The trap distribution remains as the only free parameter to describe the energetic position of the TSC peak maximum in temperature. Here, a distribution of trapping sites with according detrapping probabilities must be included in order to describe the shape of the entire TSC signal. In particular, a Gaussian trap distribution superimposed with exponential tail states is found to reproduce the TSC signal well, which is in agreement with the IS measurements. However, due to the comparably small density of tail states, the focus is on the central Gaussian trap representing the main TSC peak maximum. In total, the magnitude of the TSC is given by the overall trap density N_T and the product of mobility and lifetime $\mu\tau$ of the free holes. The former is directly correlated to the number of extracted charge carriers $N_T = \frac{Q}{A \cdot L} = \frac{\int I(t)dt}{A \cdot L}$.

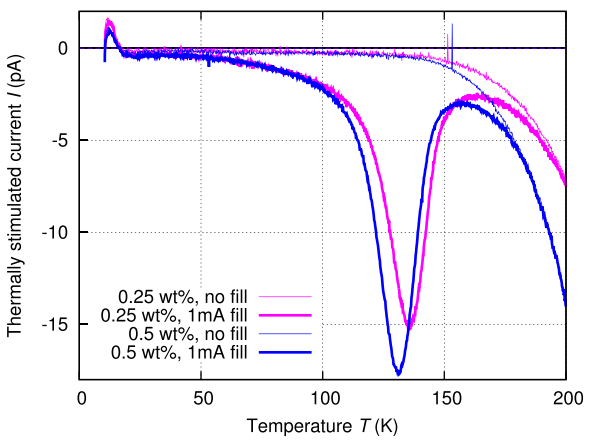

FIG. 7. TSC measurements of a ZnPc:C_{60} device with 0.25 wt % as well as 0.5 wt % p-dopant with and without a loading current ($N_G = 2.4/2.8 \times 10^{16}$ cm^{-3}, $\sigma_G = 0.016$ eV, and $E_G = 0.35/0.34$ eV, respectively).

Here, the energy of the Gaussian trap level is located at $E_G = 0.35$ eV (0.34 eV) for the 0.25 wt % (0.5 wt %) doping concentration, respectively. Hence, the trap energies obtained by TSC are reduced by about 0.06 eV as compared to the activation energies obtained from the temperature dependence of the maximum change in the capacitance (Figure 3). This effect can be related to the assumption of a constant transport model, which is necessary for evaluating the TSC data in order to limit the complexity of the problem. For instance, the change in the transport level with temperature can be estimated from Ref. 28 to be in the range of 0.1–0.2 eV between 200 and 300 K for a broad, exponential DOS, as it was previously observed for hole transport in ZnPc:C_{60} blend layers.[21] Thus, at lower temperatures, the transport level would be closer to the trap, reducing the activation energy. Since the TSC measurements are performed at lower temperatures than the IS measurements, the reduced trap energies obtained from this method are attributed to the difference in the transport level as compared to the DOOS peak determined by IS.

Furthermore, N_G of the main peak is found to be 2.4×10^{16} cm^{-3} (2.8×10^{16} cm^{-3}) for the 0.25 wt % (0.5 wt %) doped sample, respectively. Compared to N_G of the peak determined by IS, the absolute value is the same for 0.25 wt % and it is reduced by about a factor of 3 for 0.5 wt %. This difference can be explained as follows: The $\mu\tau$ product is a fitting constant that is found to be $\mu\tau = 9.6 \times 10^{-10}$ cm^2/V (0.25 wt %) and 1.25×10^{-9} cm^2/V (0.5 wt %). These values are remarkably higher than $\mu\tau = 3 \times 10^{-11}$ cm^2/V reported previously by Ray *et al.*[38] However, a comparably high electron concentration due to photoexcitation led to a diminished lifetime of free holes in neat ZnPc films. In contrast, p-doping of our samples shifts the Fermi level towards the hole transport level and creates additional free holes increasing the hole lifetime and the hole mobility. Assuming a mobility of 10^{-6} cm^2/Vs (e.g., from Ref. 39) results in a lifetime of the free charge carriers of 10^{-3} s, which is in the range of the traveling time of a free hole through the sample.[40] Therefore, it is likely that charge carriers released far away from the extraction contact do not reach the collecting interface but recombine instead. This effect is expected to be more pronounced in the device with the higher doping concentration. In addition to the uncertainties of N_t in the DOOS reconstruction, this is a possible explanation for the difference in the trap density of the 0.5 wt % doped sample obtained via thermally stimulated currents as compared to impedance spectroscopy. Altogether, the peaks observed in the TSC measurements can be attributed to one and the same trap as the Gaussian trap observed in the DOOS reconstruction from IS.

E. Solar cell characteristics

In order to investigate the effect of doping on solar cells, the current-voltage (*J-V*) characteristics of the doped devices are measured under illumination. Figure 8 presents the measurement data for the doping concentrations 0.25 wt % (magenta) and 0.5 wt % (blue) at device thicknesses of 100 nm (triangles and dashed lines) and 200 nm (circles and dotted lines). The power conversion efficiency of these devices is low (0.08%–0.27%) because the devices lack in selective transport layers providing significant built-in potential and preventing recombination at the contact. Hence, only the charge carriers generated in the depletion region are efficiently separated (by the depletion voltage V_d). Here, the short circuit current J_{SC} and the efficiency increases with decreasing device thickness and concentration. The 100 nm device with 0.25 wt % doping is most efficient, which is reasonable as it has the largest depletion region (compare Table I), particularly with respect to the overall device thickness. As only a part of the device is depleted, charge carriers generated outside the depletion region have to reach the contact by diffusion, which is inefficient and leads to recombination losses. Thus, the devices with higher doping concentration are less efficient although they have a higher V_d, but it does not compensate for the small depletion zone.

Comparing the open circuit voltage V_{OC} of all devices, those with the same doping concentration also possess the same V_{OC} as expected. Furthermore, V_{OC} is larger for the devices with the lower doping concentration. Furthermore, differences in V_{OC} equal the differences in V_{bi}, which is often estimated from the crossing point of dark and illuminated *J-V* curves (indicating zero photocurrent). This observation is in agreement with previous work on V_{bi}.[41] The absolute values of V_{bi} obtained from the photocurrent are in the range of 0.3–0.4 V, i.e., smaller than the value obtained from the Mott-Schottky analysis, but still reasonable considering the difficulties of determining V_{bi} from different methods.[42]

Apart from the low V_{OC} and J_{SC} as compared to undoped samples, the fill factors of 36%–40% are also reduced as compared to complete BHJ solar cells with this blend layer and with selective transport layers.[43] The low fill factors indicate additional recombination in the doped devices that is explained by a higher hole density due to the p-doping. Moreover, the *J-V* slope at negative voltages indicates a voltage dependence of the photocurrent due to the increasing depletion region. Here, the slope decreases with increasing device thickness and doping concentration. On the one hand, less charge carrier pairs are generated in the thicker device (per volume) causing a shallow slope, and on the other hand, in the higher doped sample more negative voltage is necessary to increase the depletion region for additional charge carrier generation.

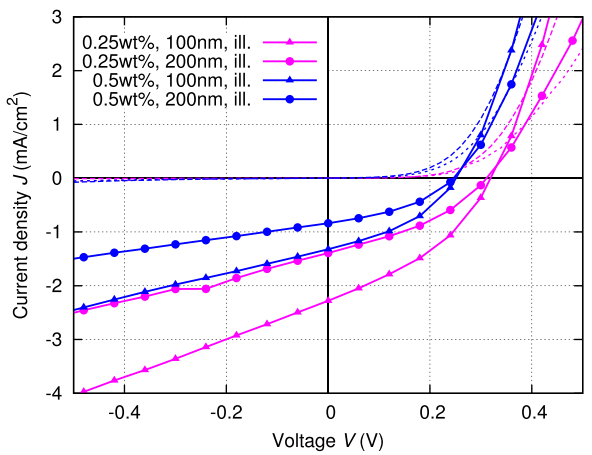

FIG. 8. Room temperature *J-V* characteristics of the doped devices measured under 1 sun illumination (solid lines with symbols) and in dark (dashed and dotted lines).

In agreement with previous studies on doped blend layers,[44] doping provides a tool for optimizing the solar cell efficiency by trap filling. However, doping is only beneficial for a solar cell if the depletion region is not much smaller than the thickness of the solar cell, as it is the case for the devices studied here. Hence, optimizing the solar cell by weak doping is a trade-off between, (i) making the device more conductive for efficient charge carrier transport, (ii) keeping a built-in potential as the driving force for charge carrier separation, and (iii) finding the optimal layer thickness where most of the light is absorbed.

F. Discussion

Deep, hole-type trap states, represented by a Gaussian-shaped peak as well as exponential tail states, were identified in the DOOS distribution reconstructed from IS measurements. Using TSC investigations of the same samples, the shape and energetic position of the Gaussian trap were confirmed. Studying the *J-V* curves of these samples under illumination, the doping concentrations used for trap filling were shown to be detrimental for ZnPc:C_{60} solar cells as they decrease the built-in potential, which is necessary to separate charge carriers effectively. In agreement with the literature,[23,24,45] the deep trap states also constitute a source of recombination losses in this blend layer. Aiming at improving the solar cell efficiency, the traps must be characterized and their origin identified. Thereby, the central question is whether the traps are externally induced by the doping or whether they are a property of the donor-acceptor blend (i.e., they are also present in the intrinsic device but not occupied) and, in this case, whether they are a property of the donor or caused by blending with the acceptor.

Regarding the influence of the dopants on the DOS, the doping process itself might cause additional states in the DOS, which can trap charge carriers, e.g., if the Gaussian trap is caused by ionized dopants that are negatively charged and act as Coulomb traps for holes.[46] However, in this case, the activation energy of the doping process obtained from the Mott-Schottky analysis should be similar to the temperature activation of the Gaussian trap. Here, the activation energy of the dopants is by a factor of 10 smaller than the trap energies found using IS and TSC. A similar Gaussian trap ($E_G = 0.6$ eV, $N_G = 1.2 \times 10^{17}$ cm^{-3}) observed in weakly p-doped pentacene was already related to the matrix since the trap concentration saturates upon increasing doping concentration.[35] Furthermore, the activation energy obtained from a Mott-Schottky analysis in that reference (54 meV)

was comparable to the one reported here. Although the present results do not show a saturation of the Gaussian trap density like in the reference, the similarity of the trap distributions and activation energies at equal molar ratios directs towards a common physical origin of the traps. Hence, it seems reasonable to conclude that the Gaussian trap observed in this work is related to the donor-acceptor blend layer and not to the doping process itself.

In the undoped sample, the trap states are not occupied and thus do not contribute to the IS signal. This observation is in agreement with previous IS measurements of this blend layer, where trap states had to be filled by illumination[23] or by charge carrier diffusion from adjacent doped layers[24] in order to give a capacitive contribution in the IS. Here, doping has proven as an elegant solution for defined trap filling. Furthermore, the energetic range of the DOOS reconstruction can be increased in future studies by extending the variation of doping concentration.

Asking whether the trap peak is related to the donor material or caused by blending of the donor with an acceptor, the results are compared to recent studies on neat layers doped with widely varied doping concentrations. A Gaussian trap was reported for neat ZnPc layers p-doped with F6-TCNNQ,[27] however, with a higher trap density ($N_G = 7.2 \times 10^{17}\,cm^{-3}$) and deeper in energy (1.2 eV off the HOMO onset, i.e., in the C_{60} LUMO of the blend layers). Nevertheless, this result does not contradict this work as this trap might be present in addition to the one found here. The trap reported in that reference is not relevant to blend layers because it would be located in the LUMO(C_{60}). Reversely, the trap found here might not be resolved in that reference since it is only present at a low density and a single Gaussian trap was assumed. Additionally, exponential tail states with a characteristic energy of $E_t = 0.157$ eV were reported,[27] in good agreement with the tail state distribution determined before in this work ($E_t = 0.14$ eV). Furthermore, the authors showed that ZnPc is efficiently doped for molar ratios (dopant/matrix) between 10^{-4} and 10^{-3}. Assuming that this result is independent of the p-dopant, the observed occupation of trap states in the devices doped with 0.07 and 0.13 mol. % as well as the obtained doping efficiencies agree very well with this reference. Altogether, the exponential trap states are suggested to be an intrinsic property of ZnPc as neat and blend layers have exponential tail states with a comparable characteristic energy.[47] The Gaussian trap reported here cannot be related to the one obtained in neat ZnPc layers before, but it might have been overseen for having a low density. Hence, neat ZnPc layers would have to be studied by IS for direct comparison, ideally using $C_{60}F_{36}$ as a p-dopant, in order to identify the origin of the Gaussian trap.

Moreover, the DOOS distribution reported here for ZnPc:C_{60} blend layers may explain the asymmetry in the Fermi level position of the intrinsic ZnPc:C_{60}, which is close to the C_{60}-LUMO level and not in the center of the energy gap: The Fermi level defines the energetic position, where the probability to find free electrons and holes is the same. If the density of free holes is reduced due to the deep hole traps, the Fermi level must shift towards the electron transport level accordingly. Hence, the Fermi level aligns close to the minimum in the DOS. In this case, this minimum is not yet reached at the deepest energies (0.6 eV) of the doped devices, in agreement with the Fermi level offset from the HOMO(ZnPc) determined by UPS (0.7–0.8 eV). Thus, combining UPS measurements with the DOOS distribution enables novel insights into the energetic position of the charge carriers relevant to the transport.

IV. CONCLUSION

In summary, the DOOS of a p-doped organic semiconductor blend layer (ZnPc:C_{60}) was determined from temperature dependent IS spectra.[25] The same samples are measured with TSC for validating the trap distribution. The DOOS distribution shows a Gaussian trap state, which is more occupied at higher doping concentrations, as well as deep, exponential tail states that compare to those previously determined in this blend layer. Being unoccupied in the undoped sample, the trap states can be filled by doping enabling a detailed trap characterization. The maximum density of the trap states with Gaussian distribution is at 0.40 eV (0.41 eV) with respect to the hole transport level, having a density of $2.3 \times 10^{16}\,cm^{-3}$ and $8.0 \times 10^{16}\,cm^{-3}$ for the 0.25 wt % (0.5 wt %) doped sample, respectively. No influence of the dopant on the DOS is found. Instead, it seems reasonable that the trap peak is related to the donor material. For solar cell efficiencies, trap filling by doping is shown to be detrimental at the concentrations used here and a pathway for optimizing a solar cell by weak doping is derived. Altogether, p-doping of blend layers facilitates insight into the hole-type DOS distribution with respect to the transport level and it reasons the asymmetry in the Fermi level position observed in this blend layer system. Future studies have to identify the trap origin and possible ways to avoid the traps in order to further improve charge carrier transport and hence the efficiency of solar cells.

ACKNOWLEDGMENTS

The authors gratefully acknowledge fruitful discussions with W. Tress as well as useful comments on the manuscript from M. Tietze. Financial support came from the ESF-NFG (orthophoto/100087862).

APPENDIX: THEORY

Electrical IS measures the current response of a device to a small, sinusoidal voltage perturbation with frequency ω that is described by the complex impedance $\boldsymbol{Z}(\omega)$

$$\boldsymbol{Z}(\omega) = |\boldsymbol{Z}(\omega)| \cdot e^{i\phi(\omega)} = R(\omega) + iX(\omega) \qquad \text{(A1)}$$

using the frequency dependence of phase $\phi(\omega)$ and amplitude $|\boldsymbol{Z}(\omega)|$ or of resistance $R(\omega)$ and reactance $X(\omega)$ in terms of real and imaginary part. Equivalently, the admittance $\boldsymbol{Y}(\omega)$ is defined by

$$\boldsymbol{Y}(\omega) = \frac{1}{\boldsymbol{Z}(\omega)} = G(\omega) + iB(\omega). \qquad \text{(A2)}$$

Here, real and imaginary part are given by the conductance $G(\omega) = \frac{R(\omega)}{R^2(\omega)+X^2(\omega)}$ and the susceptance $B(\omega) = -\frac{X(\omega)}{R^2(\omega)+X^2(\omega)}$.

Assuming a parallel *R–C* equivalent circuit, the system is described by the frequency-dependent reactance $X(\omega) = -\frac{\omega C(\omega)R^2(\omega)}{1+\omega^2C^2(\omega)R^2(\omega)}$, so that $B(\omega) = \omega C(\omega)$, and Eq. (A2) can be written as

$$\boldsymbol{Y}(\omega) = G(\omega) + i\omega C(\omega). \tag{A3}$$

Typically, the capacitance function $C(\omega)$ is composed of a frequency independent part, given by the geometrical capacitance of the device C_{geo}, as well as an additional, frequency dependent part $C_t(\omega)$, which is caused by time dependent phenomena such as trapping or transport.

Focusing on the dynamics of a discrete level trap with an activation energy E_A with respect to the transport level, the trap capacitance is characterized by a temperature dependent frequency $\omega_0(T)$ given by

$$E_A = kT \ln\frac{2\nu_0}{\omega_0}. \tag{A4}$$

Here, k is Boltzmann's constant and ν_0 is the attempt-to-escape frequency. Relation (A4) relies on the Boltzmann-type probability for a charge carrier to charge and discharge a state of energy E_A by applying a stimulus of frequency ω_0. For $\omega \ll \omega_0$, the capacitance is given by $C_{geo} + C_t$, while for $\omega \gg \omega_0$, the total capacitance is given by C_{geo}. Hence, ω_0 is defined by the inflection point of $C(\omega)$. Practically, ω_0 is typically determined by the maximum of the derivative of $-\omega dC/d\omega$.[25,48] The temperature dependence of ω_0 reveals E_A and ν_0. It can be shown that this derivative is in first order equal to the trap contribution to the device conductance $G_t(\omega)/\omega = (G(\omega) - G_{dc})/\omega$ (with the dc conductance $G_{dc} = R(\omega \to 0)/|\boldsymbol{Z}(\omega \to 0)|^2 \approx 1/R$). In this work, $G_t(\omega)/\omega$ is used to determine ω_0 for reasons explained in the text. Note that a temperature dependence of the transport level as expected in organic semiconductors[28] affects E_A.

The concept of (de-)charging a discrete level trap can be generalized to describe a trap distribution, where a state located at the demarcation energy E_ω (with respect to the transport level) can be charged and discharged by applying a small stimulus of frequency ω

$$E_\omega = kT \ln\frac{2\nu_0}{\omega}. \tag{A5}$$

If the trap distribution has a distinct maximum (and only in this case), the inflection frequency ω_0 of the trap maximum can be determined from the maximum in $\omega dC/d\omega$ or G_t/ω, equivalently to a discrete trap level. Accordingly, ν_0 follows from the temperature dependence of ω_0. Assuming that ν_0, which is obtained from the trap maximum, is valid for all energies of the distribution, the frequency spectrum of the impedance signal can be translated into an energy axis E_ω.

Moreover, according to Walter *et al.*[25] and Burtone *et al.*,[49] knowledge of the Fermi level and the transport levels enables relating the capacitive contribution of the traps to the energy resolved DOOS. While Burtone *et al.* varied the parameters of a trap with an *a priori* assumed energetic distribution for fitting the related capacitance to measured $C(\omega)$ spectra, Walter *et al.* used a simplified device energy level diagram to calculate the density of trap states directly from the $C(\omega)$ spectra. Thereby, the differential capacitance that decays over a depletion region described by a plane capacitor with a potential drop V_d can be expressed as follows:

$$\frac{1}{Ad}\frac{dC}{d\omega} = \frac{1}{Ad}\frac{e}{V_d}\frac{dq}{d\omega} \tag{A6}$$

$$= \frac{1}{Ad}\frac{e}{V_d}\frac{dq}{dE_\omega}\frac{dE_\omega}{d\omega} \tag{A7}$$

using the device area A, the depletion width d, the total stored charge density q, and the potential drop over the depletion layer V_d. The frequency change of the energy $dE_\omega/d\omega = -kT/\omega$ follows from Eq. (A5). Furthermore, the charges contributing to the capacitance dq/dE_ω constitute the density of occupied trap states distribution $N_t(E_\omega)$. Accounting for a certain charge carrier distribution depending on the shape of the depletion region (in the direction perpendicular to the substrate plane), Walter *et al.*[25] derived the following relations for DOS reconstruction for an n-i-p solar cell with hole traps obeying a linear energy level diagram and for an n^+-p^- device with a parabolic energy level diagram

$$N_t(E_\omega) = \begin{cases} -\dfrac{V_d^2}{Ad[eV_d - (E_{Fn\infty} - E_\omega)]}\dfrac{dC}{d\omega}\dfrac{\omega}{kT} & \text{(linear)} \\ -\dfrac{2V_d^{3/2}}{Ad\sqrt{e}\sqrt{eV_d - (E_g - E_\omega)}}\dfrac{dC}{d\omega}\dfrac{\omega}{kT} & \text{(parabolic)}. \end{cases} \tag{A8}$$

Here, $E_{Fn\infty}$ is the equilibrium Fermi level of the n-doped layer and E_g is the transport gap of the weakly doped layer.

[1] C. W. Tang, Appl. Phys. Lett. **48**, 183 (1986).
[2] M. Hiramoto, H. Fujiwara, and M. Yokoyama, Appl. Phys. Lett. **58**, 1062 (1991).
[3] L. J. A. Koster, Phys. Rev. B **81**, 205318 (2010).
[4] C. M. Proctor, S. Albrecht, M. Kuik, D. Neher, and T. Q. Nguyen, Adv. Energy Mater. **4**, 1400230 (2014).
[5] C. F. Woellner, Z. Li, J. A. Freire, G. Lu, and T.-Q. Nguyen, Phys. Rev. B **88**, 125311 (2013).
[6] L. J. A. Koster, V. D. Mihailetchi, and P. W. M. Blom, Appl. Phys. Lett. **88**, 052104 (2006).
[7] M. Kuik, L. Koster, G. Wetzelaer, and P. W. M. Blom, Phys. Rev. Lett. **107**, 256805 (2011).
[8] T. Kirchartz, B. E. Pieters, J. Kirkpatrick, U. Rau, and J. Nelson, Phys. Rev. B **83**, 115209 (2011).
[9] A. Foertig, A. Wagenpfahl, T. Gerbich, D. Cheyns, V. Dyakonov, and C. Deibel, Adv. Energy Mater. **2**, 1483 (2012).
[10] S. Novikov, D. Dunlap, V. Kenkre, P. Parris, and A. Vannikov, Phys. Rev. Lett. **81**, 4472 (1998).
[11] C. Tanase, E. J. Meijer, P. W. M. Blom, and D. M. de Leeuw, Phys. Rev. Lett. **91**, 216601 (2003).
[12] W. F. Pasveer, J. Cottaar, C. Tanase, R. Coehoorn, P. A. Bobbert, P. W. M. Blom, D. de Leeuw, and M. A. J. Michels, Phys. Rev. Lett. **94**, 206601 (2005).
[13] R. Coehoorn, W. Pasveer, P. Bobbert, and M. Michels, Phys. Rev. B **72**, 155206 (2005).
[14] M. L. Tietze, K. Leo, and B. Lüssem, Org. Electron. **14**, 2348 (2013).
[15] F. Bussolotti, S. Kera, K. Kudo, A. Kahn, and N. Ueno, Phys. Rev. Lett. **110**, 267602 (2013).

[16]R. Haering and E. Adams, Phys. Rev. **117**, 451 (1960).
[17]J. Schafferhans, A. Baumann, A. Wagenpfahl, C. Deibel, and V. Dyakonov, Org. Electron. **11**, 1693 (2010); e-print arXiv:1008.4230.
[18]A. G. Werner, J. Blochwitz, M. Pfeiffer, and K. Leo, J. Appl. Phys. **90**, 123 (2001).
[19]N. von Malm, R. Schmechel, and H. von Seggern, Synth. Met. **126**, 87 (2002).
[20]B. Li, J. Chen, D. Yang, and D. Ma, Semicond. Sci. Technol. **26**, 115006 (2011).
[21]J. Fischer, J. Widmer, H. Kleemann, W. Tress, C. Koerner, M. Riede, K. Vandewal, and K. Leo, J. Appl. Phys. **117**, 045501 (2015).
[22]G. Garcia-Belmonte, P. P. Boix, J. Bisquert, M. Lenes, H. J. Bolink, A. La Rosa, S. Filippone, and N. Martín, J. Phys. Chem. Lett. **1**, 2566 (2010).
[23]D. Ray, L. Burtone, K. Leo, and M. Riede, Phys. Rev. B **82**, 125204 (2010).
[24]L. Burtone, J. Fischer, K. Leo, and M. Riede, Phys. Rev. B **87**, 045432 (2013).
[25]T. Walter, R. Herberholz, C. Müller, and H. W. Schock, J. Appl. Phys. **80**, 4411 (1996).
[26]S. Khelifi, K. Decock, J. Lauwaert, H. Vrielinck, D. Spoltore, F. Piersimoni, J. Manca, A. Belghachi, and M. Burgelman, J. Appl. Phys. **110**, 094509 (2011).
[27]M. L. Tietze, P. Pahner, K. Schmidt, K. Leo, and B. Lüssem, Adv. Funct. Mater. **25**, 2701 (2015).
[28]V. Arkhipov, E. Emelianova, and G. Adriaenssens, Phys. Rev. B **64**, 125125 (2001).
[29]R. Schmechel, J. Appl. Phys. **93**, 4653 (2003).
[30]S. Mehraeen, V. Coropceanu, and J.-L. Brédas, Phys. Rev. B **87**, 195209 (2013).
[31]M. L. Tietze, W. Tress, S. Pfützner, C. Schünemann, L. Burtone, M. Riede, K. Leo, K. Vandewal, S. Olthof, P. Schulz, and A. Kahn, Phys. Rev. B **88**, 085119 (2013).
[32]H. Yoshida, MRS Proc. **1493**, 295 (2013).
[33]For an ideal semiconductor holds $E_F^i = \frac{1}{2}\left[\mathrm{EA}(C_{60}) + \mathrm{IP}(\mathrm{ZnPc}) + kT \ln\left(\frac{N_V}{N_C}\right)\right]$.
[34]R. Meerheim, S. Olthof, M. Hermenau, S. Scholz, A. Petrich, N. Tessler, O. Solomeshch, B. Lüssem, M. Riede, and K. Leo, J. Appl. Phys. **109**, 103102 (2011).
[35]P. Pahner, H. Kleemann, L. Burtone, M. L. Tietze, J. Fischer, K. Leo, and B. Lüssem, Phys. Rev. B **88**, 195205 (2013).
[36]M. L. Tietze, L. Burtone, M. Riede, B. Lüssem, and K. Leo, Phys. Rev. B **86**, 035320 (2012).
[37]H. Kleemann, B. Lüssem, and K. Leo, J. Appl. Phys. **111**, 123722 (2012).
[38]D. Ray, M. Furno, E. Siebert-Henze, K. Leo, and M. Riede, Phys. Rev. B **84**, 075214 (2011).
[39]J. Widmer, J. Fischer, W. Tress, K. Leo, and M. Riede, Org. Electron. **14**, 3460 (2013).
[40]The charge carrier traveling time perpendicular to the substrate is estimated to be $t_{\mathrm{travel}} = \frac{L}{v} = \frac{L}{\mu F} = \frac{L^2}{\mu V_{\mathrm{bi}}} = 1.8 \times 10^{-3}$ s.
[41]E. Siebert-Henze, V. Lyssenko, J. Fischer, M. Tietze, R. Brueckner, T. Menke, K. Leo, and M. Riede, Org. Electron. **15**, 563 (2014).
[42]M. Kemerink, J. M. Kramer, H. H. P. Gommans, and R. A. J. Janssen, Appl. Phys. Lett. **88**, 192108 (2006).
[43]W. Tress, A. Merten, M. Furno, M. Hein, K. Leo, and M. Riede, Adv. Energy Mater. **3**, 631 (2013).
[44]A. Veysel Tunc, A. De Sio, D. Riedel, F. Deschler, E. Da Como, J. Parisi, and E. von Hauff, Org. Electron. **13**, 290 (2012).
[45]W. Tress, K. Leo, and M. Riede, Appl. Phys. Lett. **102**, 163901 (2013).
[46]V. Arkhipov, P. Heremans, E. Emelianova, and H. Bässler, Phys. Rev. B **71**, 045214 (2005).
[47]The trap density is difficult to compare because it depends on the energy level it refers to.
[48]S. Dhariwal and B. Deoraj, Solid-State Electron. **36**, 1165 (1993).
[49]L. Burtone, D. Ray, K. Leo, and M. Riede, J. Appl. Phys. **111**, 64503 (2012).